Original Research Article

GREENHOUSE GASES SCIENCE AND TECHNOLOGY

Chemo-mechanical behavior of clay-rich fault gouges affected by CO_2-brine-rock interactions

Elisenda Bakker, Department of Earth Sciences, Utrecht University, Utrecht, Netherlands and Royal Haskoning DHV, Amersfoort, Netherlands

John Kaszuba, Department of Geology and Geophysics and School of Energy Resources, University of Wyoming, Laramie, WY, USA

Sabine den Hartog, The Lyell Centre, Heriot-Watt University, Edinburgh, UK

Suzanne Hangx, Department of Earth Sciences, Utrecht University, Utrecht, Netherlands

Abstract: The impact of long-term CO_2-brine-rock interactions on the frictional properties of faults is one of the main concerns when ensuring safe geological CO_2 storage. Mineralogical changes may alter the frictional strength and seismogenic potential of pre-existing faults bounding a storage complex. However, most of these reactions are too slow to be reproduced on laboratory timescales and can only be assessed using geochemical modeling. We combined modeling of CO_2-charged formation water and fault gouges (1–1000 years residence time, i.e. 10–10^6 pore volume flushes) with friction experiments on simulated fault gouges ($T = 22$–$150°C$; $\sigma_n^{eff} = 50$ MPa; $P_f = 25$ MPa; $V =$ 0.2-100 μm/s), having mineralogical compositions as predicted by the models. As an analogue for clay-rich caprocks overlying potential CO_2 storage sites in Europe, we used the Opalinus claystone. Our experiments showed that, although significant mineralogical changes occurred, they did not significantly change the frictional behavior of faults. Instead, initial fault-gouge mineralogy imposed a stronger control on clay-rich fault behavior than the extent of CO_2-brine-rock interactions, even under chemical conditions allowing for significant reaction. We demonstrated that the impact of mineralogical changes due to CO_2-brine-rock interactions on the frictional behavior and seismogenic potential of faults could be assessed using our combination of geochemical modeling and friction experiments. Note that a complete understanding requires evaluation of additional effects, such as that of shear velocity, effective normal stress, and other fault characteristics (maturity, shear strain). © 2018 The Authors. Greenhouse Gases: Science and Technology published by Society of Chemical Industry and John Wiley & Sons, Ltd.

Additional supporting information may be found online in the Supporting Information section at the end of the article.

Keywords: fault stability; CO_2 storage; caprock integrity; mineralogical changes

Correspondence to: Elisenda Bakker, Royal Haskoning DHV, Laan 1914 35, 3818 EX Amersfoort, Netherlands.
E-mail: elisenda.bakker@RHDHV.com
Received August 6, 2018; revised October 31, 2018; accepted November 1, 2018
Published online at Wiley Online Library (wileyonlinelibrary.com). DOI: 10.1002/ghg.1831

Introduction

One of the most promising technologies to reduce global CO_2 emissions is geological storage of CO_2, in addition to transitioning to renewable energy sources, improving energy efficiency, and reducing energy consumption. Carbon capture and storage (CCS) entails the capture of CO_2 at source, and transport to, and injection into, a suitable storage site. The main storage mechanism is structural trapping of the liquid or supercritical CO_2 phase directly underneath the caprock.[1] Over time, additional, but generally more limited, storage space can be provided by dissolution trapping of CO_2 into the formation brine,[2] residual trapping of CO_2 within the pore space[3,4] and/or mineral trapping if the host mineralogy is favorable.[5] In recent years a significant amount of research has been conducted to understand CO_2-brine-rock interactions that take place during long-term CO_2 storage in saline formations and depleted hydrocarbon reservoirs (see Kampman *et al.*[6] for a review). However, many storage sites contain, or are bounded by, faults. It has been recognized that CO_2-charged formation water can react chemically with fault minerals, thereby potentially altering fault friction behavior and creating a seismicity hazard.[7] The risk of induced seismicity due to CO_2 storage should therefore be evaluated prior to geological storage of CO_2 to mitigate anthropogenic greenhouse gas emissions.[8]

Pre-existing faults that penetrate the caprock may be reactivated during CO_2 injection and lead to seismicity if fault slip is unstable.[8,9] In the short term (i.e. during the injection period), fault slip can be induced if CO_2 injection reduces the normal stress and/or increases the shear stress acting on the fault plane. Stress changes may be caused by pore pressure changes in the fault, by the coupled poro-elastic response of the surroundings (i.e. reservoir and caprock), and by thermally induced local stress changes.[10,11]

Carbon dioxide injection and storage may also induce other chemo-mechanical processes that impact fault gouges and surrounding host rock, such as changes in rock strength and fracture toughness induced by wet supercritical CO_2,[12–14] co-injection of acid gases (e.g. H_2S and SO_2), and/or development of geochemical domains on mineral surfaces (e.g. water films) and in nano-scale pores. However, our study develops a foundational understanding of mineral behavior due to CO_2-brine-rock interaction on which detailed future studies can build.

In clay-rich caprocks that overlie proposed storage reservoirs, such interactions can involve dissolution and re-precipitation of carbonates, dissolution of plagioclase feldspar, and clay minerals (illite, chlorite, and kaolinite) and precipitation of smectite.[15,16] Mineralogical changes such as these might alter the frictional behavior of fault gouge, i.e. the wear product created by fracturing of intact host rock. A change in the frictional strength affects the ease with which a fault is reactivated, while a change in the slip stability has implications for induced seismicity. The importance of the mineralogy for the frictional behavior of fault gouge has been demonstrated by numerous experimental studies (e.g. see Ikari *et al.*).[17] Competent minerals (e.g. quartz, feldspar, carbonate and anhydrite) are known to exhibit a high frictional strength (friction coefficient, $\mu = 0.6$–0.85) and both stable and unstable behavior, whereas phyllosilicates (clay minerals and micas) are significantly weaker ($\mu = 0.2$–0.5) and predominantly frictionally stable (Fig. 1A–B[18–31]). Faults generally contain polymineralic mixtures of these competent and weak minerals, and therefore exhibit complex frictional behavior, where the strength is typically controlled by the dominant mineral(s),[32] as can also be seen in Fig. 1.

To date, a limited number of experimental studies have investigated the effects of CO_2-brine-rock interactions on the mechanical properties of reservoir rocks, caprocks, and faults, including both short-term experiments (lasting hours or days – see, e.g., Samuelson and Spiers,[33] Pluymakers *et al.*[34]) and studies investigating the effect of long-term CO_2 exposure (i.e. post abandonment of the field).[12,13,35–37] One of the challenges encountered in laboratory studies investigating the long-term effects of CO_2 exposure is the slow reaction of aluminosilicates and the storage integrity timescales required by many regulators (>10 000 years), which are typically much longer than available laboratory timescales (weeks, months or occasionally a few years; see Rochelle *et al.*[38] and references therein).

In this paper we overcome this problem by using geochemical modeling to predict mineralogical changes within faults at timescales not achievable in the laboratory. Based on previous work,[20,35,39] it is expected that frictionally weak or unstable mineral phases, such as clays or carbonates, would need to make up between 20% and 80%, respectively, of the gouge composition to significantly affect its frictional

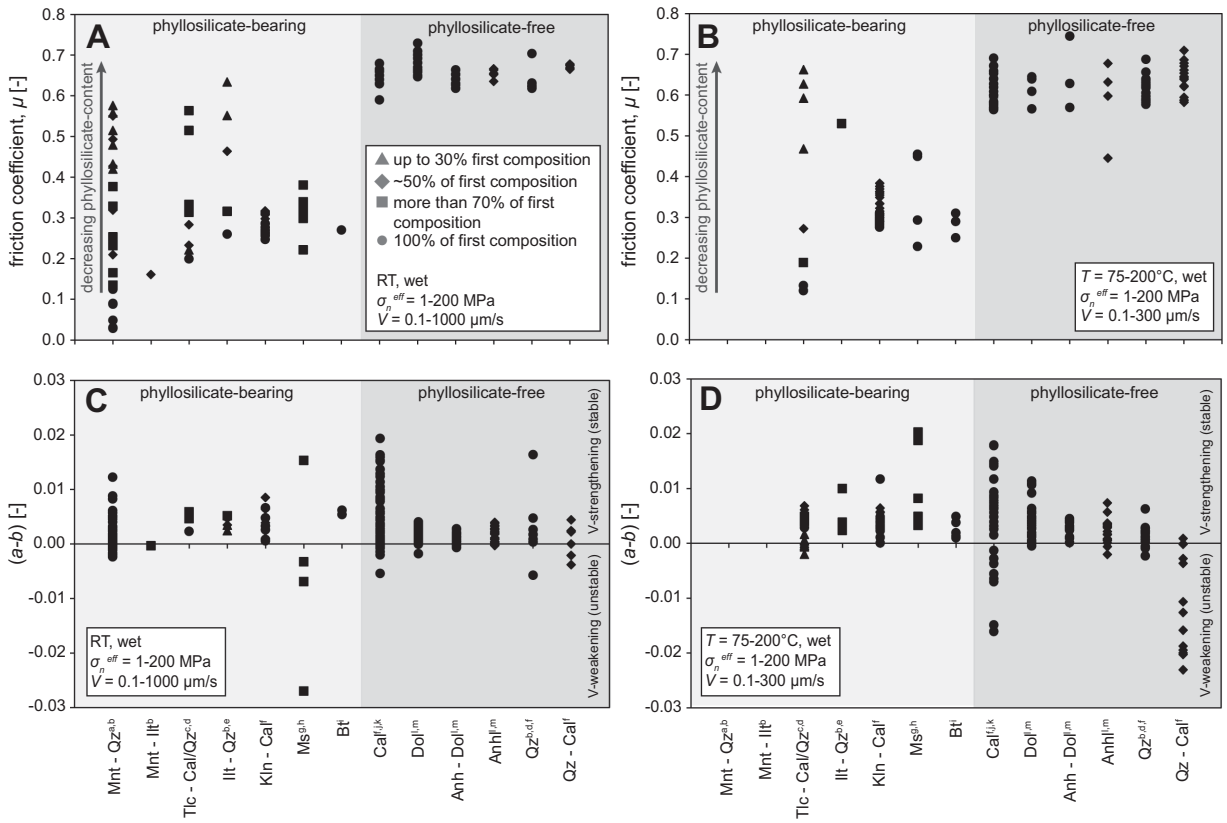

Figure 1. A and B: Friction coefficient and C and D velocity-dependence parameters as a function of mineral composition. A and C show results from experiments performed wet and at room temperature conditions, whereas B and D represent wet experiments performed at 75–200°C. Abbreviations: Mnt = montmorillonite, Ilt = illite, Tlc = talc, Kln = kaolinite, Ms = muscovite, Bt = biotite, Cal = calcite, Dol = dolomite, Qz = quartz, Anh = anhydrite.[30] [a]Ikari *et al.*,[18] [b]Tembe *et al.*,[19] [c]Giorgetti *et al.*,[20] [d]Moore and Lockner,[21] [e]den Hartog *et al.*,[29] [f]Bakker,[27] [g]Van Diggelen *et al.*,[28] [h]den Hartog *et al.*,[31] [i]Lu and He,[22] [j]Verberne *et al.*,[23] [k]Carpenter *et al.*,[24] [l]Pluymakers *et al.*,[25] [m]Scuderi *et al.*[26]

behavior. However, the complexity of the interaction between different minerals, and their relation to foliation,[40] makes it difficult to predict the exact impact of fluid-induced mineralogical changes. We therefore performed friction experiments on simulated gouges composed of the predicted mineralogy to quantify the frictional behavior of evolved fault gouges. We assessed chemical-mechanical effects of long-term CO_2-brine-rock interactions on fault gouges in a clay-rich caprock. As an analogue for clayey caprocks found overlying hydrocarbon reservoirs in sedimentary basins in Western-Europe, we use Opalinus claystone (OPA), a carbonate-bearing claystone, as the starting material. We focus on the impact of mineralogical changes on fault strength and on stable versus unstable slip behavior, which has implications for induced seismicity.

Materials and methods

Natural clay-rich material: Opalinus claystone

The material used in this study was obtained from the 'silty-shaly' facies of the Opalinus claystone, sampled at the Mont Terri Underground Rock Laboratory, Switzerland (courtesy of Swisstopo, Dr C. Nussbaum), and is representative of carbonate-bearing claystone caprock. The OPA is a Middle Jurassic, very fine-grained, low-porosity claystone consisting of homogeneously distributed fossil shells and framboidal pyrite embedded in a phyllosilicate-dominated matrix (Fig. 2). Quartz is present as non-porous, rounded grains (up to 30 μm), and calcite is present as both non-porous, rounded grains (up to 20 μm in diameter) and porous, fossil shells (varying from rounded fossils

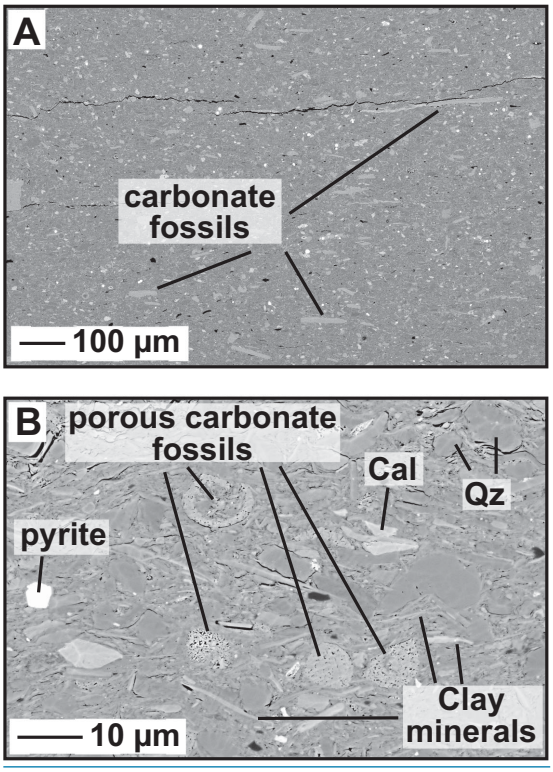

Figure 2. Scanning electron micrographs illustrating the petrography of the Opalinus claystone. A: Homogeneously distributed carbonate fossil shells embedded in a phyllosilicate-dominated matrix. B: Non-porous rounded quartz (Qz) and calcite (Cal), pyrite, and porous carbonate fossil shells.

up to several tens of microns in diameter, to elongated fossils up to 200 μm in length). Quantitative Rietveld X-ray diffraction analyses of natural OPA showed that the material consists of quartz (23 wt%), calcite (26 wt%), and minor pyrite (4 wt%), with the clay fraction consisting of chlorite (4.2 wt%), illite (5.2 wt%), illite-smectite (24.4 wt%), and kaolinite (13.2 wt%) (see the Supplementary Material, Table A1). Our measured composition is in accordance with previously reported compositions.[41]

Geochemical simulations of CO_2-brine-rock interactions in clay-rich fault rock

This study focuses on chemical-mechanical behavior induced by mineral dissolution and precipitation due to long-term CO_2-brine-rock interactions. Using Geochemist's Workbench 11.0 (GWB), the b-dot ion association model, and the resident thermo.tdat database[42] according to previously described methods,[43,44] three distinct conceptual scenarios were developed to understand how fluids rising from an underlying sandstone storage reservoir may impact chemical-mechanical processes within a faulted carbonate-bearing claystone caprock. The first scenario is a baseline scenario in which no CO_2 is injected into the underlying storage reservoir. Reservoir water that invades the fault within the overlying claystone cap is therefore not saturated with CO_2 (RW-scenario series, cf. Tables 1 and C1 of the supplementary material). In the second scenario, CO_2 is injected into the reservoir, and the reservoir water therefore becomes saturated with CO_2. Once CO_2-saturated water invades the faulted caprock, the fault is assumed to form a closed system, i.e. the fault is isolated from the underlying reservoir. The third scenario is in essence the same as the second but the fault behaves as an open system with respect to the CO_2 (but not the water) residing in the CO_2 plume present directly below the caprock, i.e. CO_2 will continue to access the fault to keep the pore fluid saturated with CO_2. Dissolved CO_2 is consumed by water-rock interactions in the closed system, whereas dissolved CO_2 is buffered and CO_2 saturation of water in the fault remains constant in the open system (C- and O-scenario series, respectively; cf. Tables 1 and C1 of the supplementary material). Details of the geochemical model and its input parameters are summarized in Appendix A of the supplementary material.

For each of these three reservoir scenarios, we approached fluid replacement within the fault by so-called fault-valve behavior,[45–47] where the fluid within the fault is periodically replaced. For the reservoir scenarios, both the fluid residence time in the fault (i.e. the time that one pore volume of reactive fluid resides in the fault rock prior to replenishment with a fresh pore volume, t_r) and total time of fluid-rock interaction within the fault (total reaction time investigated in each scenario, T_r) were varied. We simulated four residence times, 1, 10, 1000, and 10 000 years, to represent both rapid and more gradual overpressurization of the reservoir, and periodic reactivation of the fault assuming typical clay gouge permeabilities (10^{-17}–10^{-22} m^2),[48] and total time of fluid-rock interaction of 10 000 years and 1 million years. The number of pore volumes of reservoir water that passed through the fault for the duration of the simulation time (the ratio of the total time of fluid-rock interaction and the residence time, T_r/t_r) ranges from 10 to 10^6 (Table 1).

Table 1. Overview of the results of geochemical calculations performed in this study (for details see supplementary material Appendix D). Reactions among carbon dioxide, sandstone reservoir water and Opalinus shale (OPA) fault gouge were modeled for closed and open systems reacting for 10 000 years and 1 million years with residence times of 1, 10, 1000 and 10 000 years. Mineral assemblages are grouped according to crystal morphology and geomechanical properties as competent and weak phases. Closed system compositions are selected for frictional testing. Note that the mineralogy of CFOPA is not a geochemical calculation; it is Opalinus claystone from which carbonate minerals were dissolved.

Sample name	Residence time (year)	Reaction time ($\times 10^3$ years)	No. of pore volumes (-)	Quartz (wt%)	Pyrite[a] (wt%)	Calcite (wt%)	Dolomite (wt%)	Siderite (wt%)	Total carbonate (wt%)	Paragonite (wt%)	Chlorite (wt%)	Total mica (wt%)	Illite (wt%)	Kaolinite (wt%)	Saponite (smectite) (wt%)	Nontronite smectite (wt%)	Pyrophyllite (wt%)	Total clay (wt%)	Competent: weak[b]
				Competent phases						Weak phases									
Opalinus claystone: starting composition																			
Unreacted OPA			n.a.	**23**	4	26	0.0	0.0	**26**	0.0	4.2	**4.2**	29.6[c]	13.2	0.0	0.0	0.0	**42.8**	**51.0: 49.0**
Model OPA (closed system)			n.a.	**23.4**	3.6	24.7	0.6	0.0	**25.2**	0.0	4.0	**4.0**	24.7	13.5	5.5	0.0	0.0	**43.8**	**50.4: 49.6**
Model OPA (open system)			n.a.	**25.5**	3.5	19.9	8.7	0.0	**28.7**	0.0	3.8	**3.8**	23.2	13.4	0.0	0.0	0.6	**38.3**	**56.3: 43.7**
OPA exposed to reservoir water																			
RW-10-10k	10	10	10^3	**22.2**	3.9	22.2	2.6	0.0	**24.8**	11.4	0.0	**11.4**	22.7	4.8	4.6	5.7	0.0	**37.8**	**48.9: 51.1**
Carbonate-free OPA (leached)																			
CFOPA	n.a.	n.a.	-	**31.1**	5.4	0.0	0.0	0.0	**0.0**	0.0	5.7	**5.7**	40.0[c]	17.8	0.0	0.0	0.0	**63.5**	**32.8: 67.2**
OPA exposed to CO_2-saturated reservoir water under closed system conditions																			
C-10-10k	10	10	10^3	**31.0**	4.1	7.0	9.8	3.6	**20.4**	0.0	0.0	**0.0**	23.4	21.1	0.0	0.0	0.0	**44.5**	**53.6: 46.4**
C-10-1M	10	1000	10^5	**45.0**	5.1	0.0	0.0	0.0	**0.0**	0.0	0.0	**0.0**	0.0	49.9	0.0	0.0	0.0	**49.9**	**47.4: 52.6**
C-1k-10k	1000	10	10	**26.4**	3.5	19.9	8.5	3.2	**31.6**	0.0	0.0	**0.0**	21.1	17.4	0.0	0.0	0.0	**38.5**	**60.1: 39.9**
C-1k-1M	1000	1000	10^3	**35.0**	4.0	6.0	12.5	3.6	**22.2**	0.0	0.0	**0.0**	0.0	38.8	0.0	0.0	0.0	**38.8**	**59.6: 40.4**

[a]For the simulated gouge compositions pyrite was not incorporated. During preparation of the gouges, the wt% of each phase was adjusted accordingly to account for this.
[b]Pyrite was not taken into account for this ratio and it was adjusted accordingly.
[c]OPA consisted for 5.2% of illite and 24.4% of illite-smectite clay. CFOPA consisted of 7.0% of illite and 33.0% of illite-smectite clay (see also Table A1 of the supplementary material).
n.a. = Not applicable.

In our evaluation of the modeling results, we grouped the various minerals in the gouge according to four main mineral groups, depending on hardness and crystal morphology: quartz, carbonates (calcite, dolomite, siderite), micas (chlorite, paragonite), and clay minerals (illite, smectite, kaolinite). Note that, due to limitations of geochemical models and experimental methods, we treated interlayer illite-smectite as a mixture of end-member illite and smectite in appropriate proportions (i.e. 80% illite, 20% smectite, cf. Table A1). We do not expect this approach to affect our geochemical modeling results or the frictional properties of our simulated gouges significantly (cf. Moore and Lockner).[49]

Sample preparation

All friction experiments were performed on finely powdered OPA or mineral mixtures. Intact natural materials and individual minerals were crushed using a mortar and pestle, and sieved to a grain size of $<35\ \mu$m. For selected compositions (Table 1), powders of quartz (99.9% pure; Beaujean quartz sand), kaolinite (100% pure; Merkx®), muscovite (90% muscovite plus ~10% quartz impurities for which no correction was made; commercially obtained), calcite (Iceland spar[23]), dolomite (97% dolomite plus ~3% labradorite; Forno–Apuan Alps), and illite-rich shale (Rochester shale, 65% illite plus 35% quartz impurities[29]) were mixed by weight and thoroughly stirred to ensure a homogeneous mixture. Siderite, Ca-nontronite, and paragonite were difficult to obtain; analogue minerals – respectively dolomite, Ca-montmorillonite, and muscovite – were used instead. Pyrite was omitted due to its small proportion in OPA and the mineral proportions were corrected accordingly.

In addition to using mineral mixtures, a carbonate-free OPA (CFOPA) was prepared by exposing crushed OPA to an excess of acetic-acid ($C_2H_4O_2$; pH 3, at ~20-80°C), effectively removing any naturally present carbonate. After this dissolution process, the material was washed with demineralized water, dried, and sieved again ($<35\ \mu$m).

Intact, natural OPA possesses a broader range of grain size than the prepared gouges, with calcite fossils of up to 200 μm in size (see Fig. 2). However, these larger calcite clasts will most likely be crushed during fault gouge formation in nature.[50] The prepared gouges therefore have a size range typically observed in both simulated and natural fault gouges.[51]

Experimental apparatus, procedure and data processing

Frictional sliding experiments were performed using a rotary shear apparatus, as previously described by Niemeijer *et al.*[52] and den Hartog *et al.*[31] For the experiments, a ~1 mm thick ring-shaped gouge layer (inner radius 11 mm, outer radius 14 mm) was sandwiched between two roughened pistons. Under constant effective normal stress (σ_n^{eff}) and pore fluid pressure (P_f – distilled water, fully saturated conditions), the layer could be sheared at a constant rate, while the generated shear stress (τ) was measured externally.

A total of eight friction experiments were performed ($\sigma_n^{eff} = 50$ MPa, $P_f = 25$ MPa), each successively at room temperature (~22°C), 100°C and 150°C. The temperature range investigated is relevant for the depth range of potential CO_2 storage reservoirs and includes the transition from stable to unstable frictional behavior at 100–150°C as observed for calcite.[23] Note that due to this temperature-stepping approach, thermal expansion of the apparatus prevented us from measuring the compaction or dilation behavior of the gouge accurately. At each of the three temperatures, sliding was initiated at 5.43 μm/s, followed by a velocity stepping sequence (0.22–1.086–10.86–1.086–3–10–30–100 μm/s) to investigate the velocity-dependence of friction of the gouge material, reaching a total (corrected) displacement of ~33–34 mm. After velocity stepping at 150°C, a normal stress-stepping sequence (50, 60, 80 and 100 MPa for 2 mm per step, sliding velocity of 10 μm/s) was performed to determine gouge cohesion.

Shear displacement (resolution $\pm$ 1 μm, respectively), normal force ($\pm$ 0.05 kN), torque (0.1% of full scale; 1.2 N), pore fluid pressure ($\pm$ 0.015 MPa), and sample temperature ($\pm$ 1–2°C) were logged. Torque and normal force were corrected for predetermined seal friction to obtain the shear stress at a radius of 12.5 mm and effective normal stress acting on the gouge layer, whereas the shear displacement was corrected for machine stiffness (distortion). The apparent friction coefficient μ ('friction coefficient' hereafter) was calculated as the ratio of shear stress to effective normal stress, $\mu = \tau/\sigma_n^{eff}$, effectively ignoring cohesion.

The velocity dependence of μ was interpreted in the framework of rate-and-state dependent friction theory[53–55] (RSF) and expressed in terms of (a–b) (for details see Appendix B of the supplementary material).

Greenhouse Gas Sci Technol. **9**:19–36 (2019); DOI: 10.1002/ghg

In essence, if the friction coefficient μ increases following an increase in sliding velocity, the fault will slip stably, i.e. the fault exhibits 'velocity-strengthening' behavior and the accelerating slip needed for seismogenesis cannot occur. This is typically characterized by a positive $(a–b)$-value.[56] However, if μ decreases with increasing velocity, the fault has the potential to yield unstable behavior, indicated by negative $(a–b)$ values.[56] This is called 'velocity-weakening' behavior and it is expressed during the experiment as possible repetitive stick-slip events or seismogenic slip, provided that the elastic stiffness of the loading system falls in the right range.[53] Errors for $(a–b)$ are generally on the order of ± 0.001, but may be as high as ± 0.0028, depending on the quality of the fit made to the velocity-stepping data to derive the RSF-parameters (see Niemeijer and Vissers,[57] and Appendix B of the supplementary material).

Microstructural preparation and analysis

The experiments were terminated by halting shearing, cooling down the setup, and removing the pore pressure and normal stress. Upon removal from the ring shear apparatus, the sample assembly was dried at 50°C for at least 24 hours. Retrieval of the sample from the assembly led to the partial disintegration of the ring-shaped gouge layer into platy fragments. The larger fragments were cast into resin. Thick sections were prepared manually, perpendicular to the shear direction, and analyzed using a scanning electron microscope (SEM). To ensure careful polishing of the sections, we used a focused ion beam (FIB-SEM) to ion-mill the section surface, without distorting the sample surface. The SEM analysis was executed in backscatter electron (BSE) mode, to provide the best contrast between the various mineral phases.

Results and discussion

Mineral assemblages for the simulated fault gouge infiltrated by CO_2-free reservoir water and CO_2-saturated water are summarized in Table 1 and Appendix C of the supplementary material; the temporal evolution of simulated gouge compositions is provided in Appendix D of the supplementary material. The selection criteria for the mineral compositions tested in the friction experiments are: (i) > 5 wt% difference per mineral group (quartz, carbonates, mica, clay minerals) and/or (ii) > 5 wt% change in competent (quartz + carbonates) versus weak phase (mica + clay) ratio (Table C1). The scenario with the smallest mineralogical change was selected in the case of roughly similar mineralogical changes, representing the minimal impact of mineralogical changes on frictional behavior. Note that the preparation of simulated gouges with compositions similar to natural gouges has been shown to introduce an error of less than 10% in frictional strength,[58] making the approach ideal for assessing the impact of long-term fluid-rock interactions in faults.

As a baseline for evaluating the effect of CO_2 exposure on the frictional behavior of OPA, one scenario of a fault gouge infiltrated with CO_2-free reservoir water was selected for experimental investigation (cf. Table 2). From the CO_2-saturated water scenarios, we selected a total of four compositions that showed mineralogical changes significant enough to influence the frictional behavior of the gouge (Table 1). CO_2-brine-rock reactions significantly enhanced porosity in open-system simulations, whereas in closed-system simulations porosity remained more-or-less constant. However, similar mineral assemblages developed in both sets of simulations for a given residence time and total reaction time (Table C1, supplementary material). As porosity change cannot be accounted for in the type of experiments presented here, only closed-system simulated gouges were tested. We compare modeling and frictional testing results to the measurements on natural OPA to evaluate the effect of reaction with (CO_2-saturated) reservoir water on mineralogy and how such alterations affect frictional behavior.

The key results of the friction experiments on gouges with selected compositions are listed in Table 2 and shown in Figs 3 and 4. Individual values for $(a–b)$, a, b and D_c are shown in Table B1 of the supplementary material, and the $(a–b)$ values are visualized in Fig. 4D as a function of composition. In general, friction coefficient versus displacement graphs show an initial increase in μ with shear displacement, followed by either a peak strength and successive drop in μ or by yielding, often with subsequent strain hardening (Fig. 3A and B). Near steady-state sliding behavior is achieved after ~2–4 mm displacement at each temperature. Strain hardening is suggested to be related to preferential extrusion of relatively weak phyllosilicates from the unconfined sample assembly.[59] The effect of this experimental artefact is still

Table 2. List of experiments and key data. μ = (apparent) friction coefficient at displacements of 4.0, 14.7 and 25.4 mm at room temperature, 100 and 150°C, respectively. μ_i = internal friction coefficient, S_o = cohesion, as determined from linear fits to the data in Fig. 3C and D. For negative (*a–b*) values, the temperature at which this behavior was observed is indicated between brackets.

			μ (at a shear displacement of *D* mm) (–)					
Sample name	Residence time (year)	Reaction time ($\times 10^3$ years)	Room T (4.0)	100°C (14.7)	150°C (25.4)	μ_i (–)	S_0 (MPa)	+ve or –ve (*a–b*) (–)
OPA starting material								
OPA	n.a.	n.a.	0.35	0.35	0.36	0.33	0.8	+
OPA exposed to reservoir water								
RW-10-10k[a]	10	10	0.39	0.43	0.47	0.47	–1.6	+
Carbonate-free OPA								
CFOPA	n.a.	n.a.	0.28	0.28	0.30	n.d.	n.d.	+
OPA exposed to CO_2-saturated reservoir water (closed system)								
C-10-10ka[b]	10	10	0.43	0.47	0.52	0.44	2.2	–(100–150°C)
C-10-10kb[b]	10	10	0.47	0.50	0.54	0.55	–1.8	–(150°C)
C-10-1M	10	1000	0.42	0.45	0.49	0.39	4.0	–(100–150°C)
C-1k-10k	1000	10	0.40	0.43	0.46	0.47	–1.8	–(150°C)
C-1k-1M	1000	1000	0.44	0.46	0.48	0.44	2.2	–(100–150°C)

[a]Sample was over-compacted during the application of normal stress.
[b]A shear experiment with composition C-10-10k was repeated to test for reproducibility.

minimized for friction coefficients reached at relatively small shear displacements of 4.0, 14.7 and 25.4 mm at room temperature, 100 and 150°C, respectively (Fig. 4A). However, for completeness, we have also visualized the friction coefficients measured prior to each velocity step (Fig. 4B).

In the calculation of the friction coefficient, gouge cohesion is ignored (see section on 'Experimental apparatus, procedure and data processing'). To determine whether this assumption is justified, shear stress is plotted against the effective normal stress that was applied in the normal stress stepping sequence (Fig. 3C–D). The data can be described by a linear relationship of the form $\tau = S_0 + \mu_i \cdot \sigma_n^{eff}$, where μ_i is the internal coefficient of friction and S_0 is the gouge cohesion. Cohesion was mostly less than 2.2 MPa, though negative values for the cohesion were also obtained (up to –1.8 MPa). This suggests that the error in fitting a straight line to our τ vs. σ_n^{eff} data is relatively large, probably due to the extrapolation from > 50 MPa σ_n^{eff} down to zero. It is therefore not possible to correct for cohesion accurately. However, cohesion was mostly < 10% of the shear stress for our experiments, except for C-10-1M where it was 4.0 MPa, (~25–30% of the shear strength), supporting our use of an apparent friction coefficient (see [31,35,57]).

Effect of interaction with CO_2-free reservoir water

For the natural OPA, the friction coefficient shows a weak increase with sliding velocity and shear displacement, and a negligible effect of temperature, reaching values of 0.34–0.40 at room temperature and 100°C (average value of 0.37), and 0.34–0.42 at 150°C (average value of 0.38), respectively (Table 2; Figs 3A and 4A–B). Natural OPA also shows positive (*a–b*) values, i.e. velocity-strengthening behavior (Fig. 4C–D), typical for wet, carbonate-bearing, clay-rich fault gouges (e.g. Chen *et al.*).[60]

In most scenarios, reactions between CO_2-free reservoir water and OPA fault gouge begins to dissolve calcite, chlorite, illite, and kaolinite and precipitate mica and smectite (Table 1 and Appendix C in the supplementary material). In two scenarios, frequent

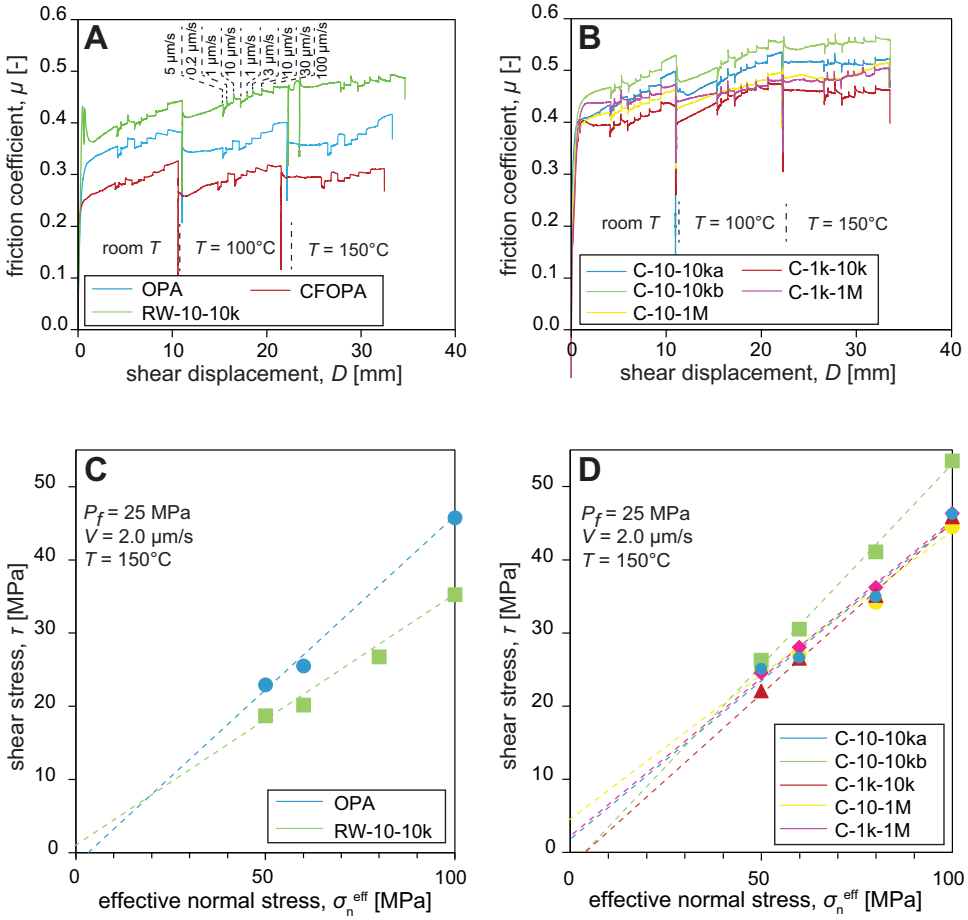

Figure 3. Typical evolution of friction coefficient with shear displacement obtained in the present experiments performed at $\sigma_n^{eff} = 50$ MPa, $P_f = 100$ MPa and room temperature, 100 and 150°C. Sliding velocity is varied from 0.22 to 100 μm/s, as indicated at 100°C for RW-10-10k. A: Friction curves for OPA, carbonate-free OPA (CFOPA) and the modeled composition for natural OPA exposed to reservoir water (RW-10-10k). B: Friction curves for selected model scenarios, assuming interactions between natural OPA and CO_2-saturated reservoir water. Peak or yield values of the shear stress obtained during the normal stress stepping sequence (not shown in A and B) as a function of effective normal stress for C: natural OPA and RW-10-10k, and D: for selected closed systems scenarios reacted with CO_2-saturated reservoir water.

replacement of reacted pore water with fresh reservoir water ($t_r = 1$–10 years, 10^5–10^6 pore volumes) completely dissolves both calcite and illite and precipitates kaolinite and a much larger amount of smectite (39–72 wt%; saponite plus nontronite content) within the fault after 1 million years (cf. RW-1-1M and RW-10-1M). As a result, these latter compositions are clay dominated (> 80 wt% clay), which will largely control their frictional behavior, as seen in previous studies (e.g. see Tembe *et al.*[19]). Therefore, and given the similarity in composition between the majority of the modeled results (RW-10-10k, RW-1k-10k, RW-1k-1M, RW-10k-10k, and RW-10k-1M), we have only selected RW-10-10k for frictional testing. With μ-values of 0.39, 0.43 and 0.47, at room temperature, 100°C and 150°C, respectively, the OPA-reservoir water scenario RW-10-10k suggests an 11–31% increase in the friction coefficient within 10 000 years, despite a 2 wt% decrease in total frictionally competent phases (quartz + carbonates – see Table 1). The velocity dependence of friction showed a small decrease in (a–b) values for RW-10-10k compared to the natural OPA sample, although values are still positive (Fig. 4C–D).

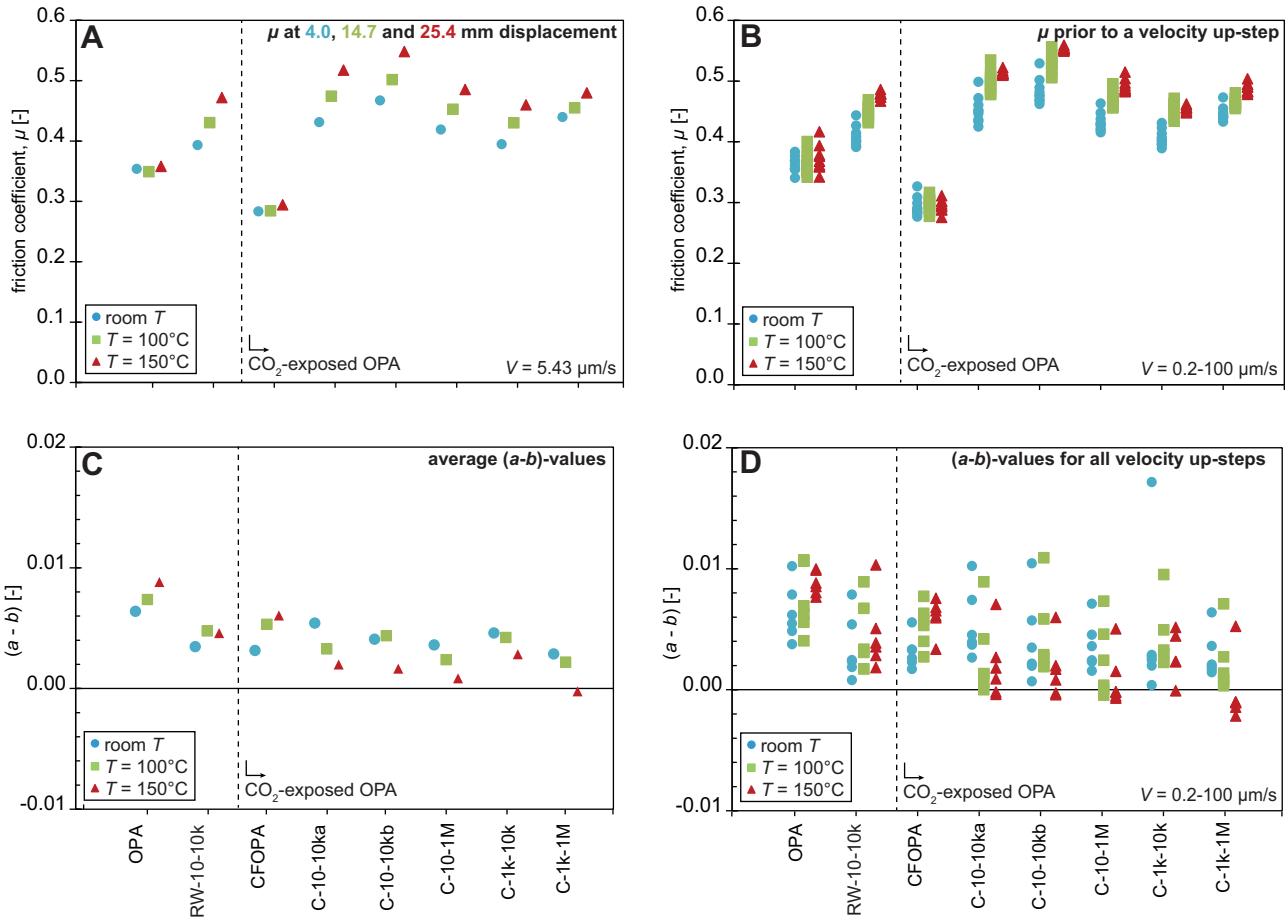

Figure 4. A: Friction coefficient at 4.0, 14.7 and 25.4 mm displacement and B: friction coefficient prior to a velocity up-step both as a function of temperature for the different compositions ($\sigma_n^{\text{eff}} = 50$ MPa, $P_f = 25$ MPa and room temperature, 100 and 150°C – see Table 1 for compositions). C: Average velocity-dependency (*a–b*) and D: velocity-dependency (*a–b*) for all velocity up-steps again as a function of temperature for the different compositions tested. From previous discussions: steady-state was not really achieved for some velocity steps.

Effect of interaction with CO_2-saturated reservoir water

Overall, simulated CO_2-exposed gouge compositions showed that the μ-values increased with increasing temperature and shear displacement, whereas (*a–b*) decreased with increasing temperature (cf. Figs 3 and 4), at the same relative displacement compared to unreacted OPA. In terms of mineralogical changes, CO_2-saturated reservoir water dissolves nearly all carbonates and micas for three scenarios in which fresh fluid frequently replaces reacted pore water within the gouge, $t_r = 1$ year for 10 000 years and 1 million years reaction time (10^4 and 10^6 pore volumes) and $t_r = 10$ years for 1 million years reaction time (10^5 pore volumes) (Table 1 and Appendix C in the supplementary material). The resulting mineral assemblage is essentially a quartz-clay gouge similar to carbonate-free OPA (CFOPA). The CFOPA showed near-temperature-independent friction coefficients of 0.28-0.30 (Table 2), i.e. 17–20% lower than for natural OPA and 28–36% lower than for reservoir water-reacted OPA (RW-10-10k; cf. Figs 3A and 4A–B). Given that CFOPA contains only 31% quartz as opposed to ~50% quartz plus carbonate for natural and reservoir water-reacted OPA, this behavior is consistent with that typically seen for gouges consisting of a mixture of weak phyllosilicates and competent quartz and/or calcite. Notably, a decrease in μ similar in magnitude to that found here has been reported for an increase in the phyllosilicate phase from ~25% to 50%, as the stress-supporting framework of quartz and/or carbonate clast changes to a

phyllosilicate-dominated matrix embedded with disperse clasts.[19–21] Values of (a–b) for CFOPA are positive and within the range measured for the reservoir water-reacted OPA and only slightly lower than those for natural OPA (Fig. 4C–D). For longer residence times (fewer pore volumes), CO_2-saturated reservoir water dissolves micas and increases quartz and clay content within the OPA fault gouge, although the detailed mineralogical evolution of the simulated gouges is complex (Table 1 and Appendixes C and D of the supplementary material). Overall, for $t_r = 10$ years (10^3 and 10^5 pore volumes; C-10-10k, C-10-1M, respectively) the total weak phase decreases by up to 3%, whereas for $t_r = 1000$ years (10 and 10^3 pore volumes; C-1k-10k and C-1k-1M, respectively) it decreases by ~10%. All four simulated gouge compositions showed μ-values increasing with temperature and shear displacement (cf. Fig. 3B and 4A–B), reaching values in the range 0.40–0.54, i.e. 14–50% higher than OPA and up to 21% higher than reservoir water-reacted OPA, when comparing values reached at the same temperatures in these experiments. Regarding the velocity dependence, a weak trend is seen from generally positive (a–b) values at room temperature, towards near zero (a–b) values at 100°C and finally slightly negative (a–b) values at 150°C, particularly at low sliding velocities ($V \leq 10$ μm/s), suggesting a transition towards more unstable type behavior with increasing temperature (see also Table B1 and Fig. B2 in the supplementary material). Note, that the observed repeatability of μ for composition C-10-10k is within ~0.03, which agrees with the reproducibility seen previously for this machine (unpublished data, SAM den Hartog – cf. Fig. 4B, D).

The relationship between frictional behavior and microstructure

Scanning electron microscopy images (backscatter electron mode) of samples C-1k-10k and C-1k-1M, representing end-member samples in terms of their quartz: carbonate ratio (26:32 and 35:22 respectively – see Table 1) show different internal deformation features (Fig. 5). Sample C-1k-10k (Fig. 5A–B) appears to be homogeneously deformed, with intact quartz grains randomly distributed throughout the gouge layer. On the other hand, hardly any intact calcite grains, which are the predominant and clearly observable phase of carbonate, remain within the body of the gouge layer. Finely crushed calcite is observed (Fig. 5B), particularly surrounding larger quartz grains, aligned along the R_1-direction. Throughout the body of the sheared gouge, large, fractured, but not crushed calcite grains are observed. This grain-fracturing is absent in the starting material (see the relatively undeformed portions of the gouge at the top and base of the image). Overall, it can be seen that, although extensive fracturing of the calcite grains is obvious, it has not led to the complete pulverization of the carbonate phase. This microstructure is in contrast to the more quartz-rich gouge (C-1k-1M; Fig. 5C–D), which still contains large quartz grains. However, the large quartz grains are embedded in a very fine-grained matrix of crushed carbonate, fragmented quartz grains, and clay particles, and no recognizable intact carbonate grains can be observed.

As stated above, the observed frictional behavior of fault gouges is assumed to depend on the fraction of frictionally weak phases present in a gouge (Table 1 and Fig. 4; see also Tembe *et al.*).[19] This typical behavior of polymineralic gouges roughly explains the observations for OPA and CFOPA but it fails to account for smaller differences in the friction coefficient such as those seen for C-10-10ka/b and C-1k-1M versus RW-10-10k and C-1k-10k (Fig. 5), the former showing systematically higher friction coefficients. It should be noted that frictionally stronger samples are characterized by higher quartz: carbonate ratios. Based on the microstructural observations, we speculate that the frictional behavior may also depend on the proportion of quartz versus carbonates in the competent phase, which influences the frictional behavior of a gouge during shearing. Our microstructural evidence suggests that the gouges with proportionally higher quartz content will generate a larger fraction of finer grained carbonate material. This is most likely caused by the preferential fracturing of calcite grains along the main cleavage plane (c-axis) over that of conchoidal fracturing of quartz.[61,62] This cleavage weakens the calcite grains, leading to an overall reduction in the carbonate grain size compared to quartz, impacting the frictional behavior, potentially aided by dissolution-induced grain-size reduction. The smaller size of the carbonate grains promotes thermally activated compaction behavior through dislocation glide and/or diffusion, resulting in a lower frictional resistance and potentially velocity-weakening behavior as observed in these samples at higher temperatures. This velocity-weakening behavior is in line with the behavior seen for pure calcite at 100–150°C.[23]

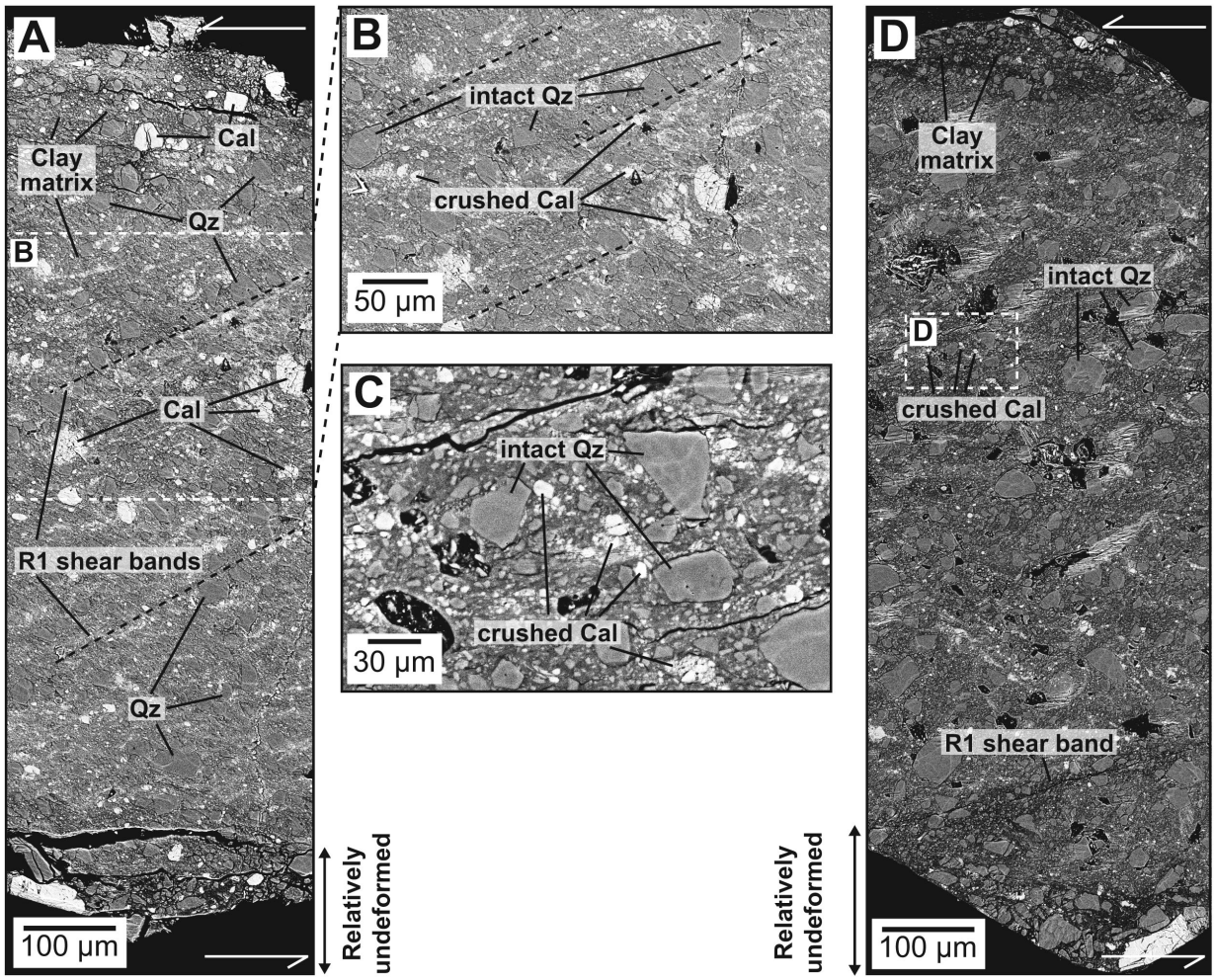

Figure 5. Scanning electron micrographs (BSE-mode) illustrating the microstructure of sheared, simulated fault gouges. A: The sheared C-1k-10k sample, consisting of 20% calcite and 12% of dolomite and siderite grains, shows crushed calcite (± siderite; white) next to intact and larger quartz grains, as well as fractured but not crushed calcite grains, all throughout the body of the gouge layer. Crushed calcite appears to form R1-shear bands. Note that the boundary shear zones are not fully developed. B: Inset of (A), showing part of the main body with distributed intact quartz next to internally fractured and crushed calcite grains. C: Sheared C-1k-1M sample, consisting of 6% of calcite and 16% of dolomite and siderite, showing some intact coarse quartz grains embedded in a matrix of clay and crushed calcite (white) and crushed quartz grains. Calcite appears to align along the R1-shear band orientation. Note the absence of a very distinct boundary shear zone. D: Inset of (C), showing significantly reduced calcite next to large quartz grains.

Impact of CO_2-brine-rock interactions on frictional behavior of clay-rich faults

The extent of reaction in CO_2 storage systems is controlled on one hand by the initial (i.e. pre-CO_2-exposure) mineralogy[58] and on the other hand by the fluid: rock ratio, i.e. the rock porosity and fluid flux through it.[36,63] For a range of fluxes of CO_2-saturated brine, geochemical modeling of the porous Opalinus claystone fault gouge showed a complex mineralogical evolution, including dissolution of carbonate minerals and precipitation of phyllosilicates and quartz, not seen in the presence of reservoir brine alone (see Fig. 6A). All four CO_2-reacted mixtures show that the mineralogical changes due to long-term CO_2-brine-rock reaction result in a roughly similar increase in frictional strength and a decrease in frictional stability with respect to the original OPA material (cf. Table 2, and

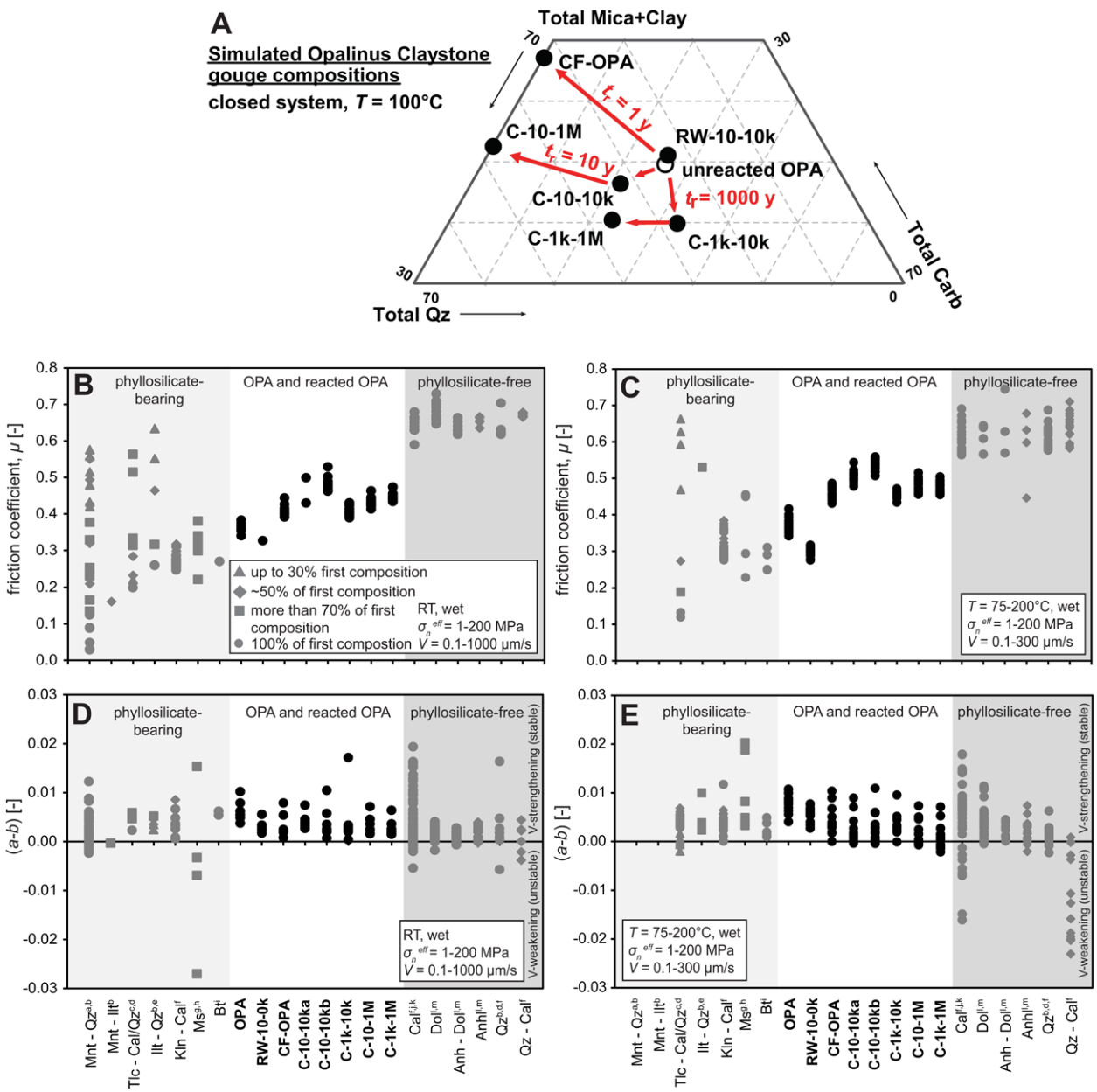

Figure 6. A: Ternary diagram illustrating the mineralogical changes occurring in natural Opalinus claystone fault gouge in response to exposure to reservoir water with and without CO_2 (closed system, $T = 100°C$). B and C: Friction coefficient, and D and E: Velocity-dependence parameters as a function of mineral composition, including OPA and reacted OPA (cf. Tables 1 and 2). B and D show results from experiments performed wet and at room temperature conditions, while C and E represent wet experiments performed at 75–200°C. Abbreviations: Mnt = montmorillonite, Ilt = illite, Tlc = talc, Kln = kaolinite, Ms = muscovite, Bt = biotite, Cal = calcite, Dol = dolomite, Qz = quartz, Anh = anhydrite.[30] [a]Ikari *et al.*,[18] [b]Tembe *et al.*,[19] [c]Giorgetti *et al.*,[20] [d]Moore and Lockner,[21] [e]den Hartog *et al.*,[29] [f]Bakker,[27] [g]Van Diggelen *et al.*,[28] [h]den Hartog *et al.*,[31] [i]Lu and He,[22] [j]Verberne *et al.*,[23] [k]Carpenter *et al.*,[24] [l]Pluymakers *et al.*,[25] [m]Scuderi *et al.*[26]

Figs 3 and 4); i.e., based on our results, the ease of fault reactivation as determined by the friction coefficient and the stability of sliding governed by $(a–b)$ are not significantly affected by CO_2-brine-rock interaction. Compared to brine-rock interactions, it can be inferred that, in the presence of CO_2-rich brine, the extent of reaction-producing secondary minerals, with frictional behavior significantly different from the primary

minerals, was not significant enough to impact frictional behavior drastically. Similar chemo-mechanical behavior has been seen in gouges derived from reservoir rock taken from natural CO_2 fields (unexposed and CO_2-exposed Entrada Sandstone, Green River, UT, USA[35] and Röt Fringe sandstone, Werkendam, Netherlands.)[36] These observations suggest that the initial mineralogy of the fault gouge (and local variations therein) imposes a stronger control on fault behavior than the extent of CO_2-brine-rock interactions, even after multiple pore volume flushes.

Furthermore, our geochemical simulations have shown that mass loss in an open fault system leads to significant porosity changes within the gouge (see Appendix D of the supplementary material). Such high gouge porosity will probably not be maintained over time. Compaction of the gouge will result in relaxation of the stress state in the surrounding host rock. Assuming a fully elastic response of the host rock and taking realistic values for the Young's modulus (in the range 2.7–8.2 GPa),[64] this stress relaxation will be concentrated in the first few centimeters surrounding the fault plane for depths relevant to CO_2 storage (>1.5 km depth).

Given the above, predicting changes in the frictional behavior, and more specifically the seismogenic potential, i.e. positive or negative (a–b) values, of a fault on the basis of mineralogical changes is certainly no easy feat. Typically competent minerals show friction coefficients of ~0.6–0.85 and phyllosilicates ~0.2–0.5, and our modeled polymineralic fault gouges fit in that trend (see Fig. 6B–C[18–31]). However, such a trend is not visible for (a–b), as the latter depends on many factors, including mineralogy (Fig. 6D–E), but also shear velocity, effective normal stress, and shear strain.[17] All these factors hinder the establishment of a definitive relationship between composition, μ and (a–b), although rough trends can be discerned (Fig. 6B–E).

What is evident is that ductile minerals, such as carbonates and sulfates, can potentially lead to velocity-weakening behavior (i.e., unstable sliding), particularly at elevated temperatures.[23,26,34] Carbonates exhibit velocity weakening under both dry and wet conditions ($T > 75$–$80°C$[23,26,35]). Furthermore, studies have shown that swelling clay minerals, like smectite, are known for their very low frictional strength ($\mu =$ 0.1–0.3, see montmorillonite data in Fig. 6B–C[18]). The presence of smectites, or precipitation thereof due to CO_2 exposure, can therefore lead to a reduction in the frictional resistance of the fault, making fault reactivation easier.

Although the impact of carbonates and/or smectites on friction and fault stability cannot be assessed accurately, it has been shown that the presence or formation of these minerals needs to be taken into account during site selection. However, such minerals would have to be present in quantities in excess of 20–40% to significantly impact fault behavior.[19,35] Such quantities would be difficult to achieve by CO_2-brine-rock interactions alone given the low reactive capacity of most typical rock types considered for CO_2 storage sites. It should be noted that, with displacement, an internal fabric with throughgoing foliation might develop, potentially controlling the frictional behavior. Such a foliation may consist of a frictionally weak mineral and it could require as little as 4 wt% of material to create this weak-mineral foliation.[40] By contrast, in the event that carbonate-rich fluids, such as those produced by (local) carbonate dissolution, migrate up-fault and depressurize, CO_2 outgassing may take place, leading to large-scale carbonate precipitation impacting fault behavior (see also Bakker *et al.*).[35] Successful and safe CO_2 storage also requires maintenance of the sealing integrity of faults in the caprocks overlying storage reservoirs. Understanding of permeability change of the gouges with progressive CO_2-induced alterations is needed to evaluate the sealing potential of faults, which was not investigated in the current experiments.

Conclusions

We assessed how the chemical-mechanical effects of long-term CO_2-brine-rock interactions affect fault frictional behavior and stability in a clay-rich caprock. We employed Opalinus claystone as an analogue for clay-rich caprocks overlying typical reservoirs considered for CO_2 storage in Western Europe. Using geochemical modeling, we predicted mineralogical changes within the fault rock at timescales not achievable in the laboratory (10 000 years to 1 million years; 10–10^6 pore volume flushes). Subsequently, the frictional behavior of selected, evolved fault gouges was tested through friction experiments ($T = 22$–$150°C$; $\sigma_n^{eff} = 50$ MPa; $P_f = 25$ MPa; $V = 0.2$–100 μm/s) on simulated gouges prepared according to the predicted mineralogical compositions. Our main conclusions are as follows:

- The frictional behavior of simulated fault gouge, prepared from natural Opalinus claystone, shows friction coefficients of ~0.35–0.42 for temperatures ranging from room temperature to 150°C. Under all conditions, the gouges show velocity-strengthening behavior, meaning stable sliding upon slip acceleration. Modeled reaction with CO_2-free reservoir water shows little variation in mineralogy but measured friction coefficients of the accordingly prepared gouge mixtures are ~10–30% higher than for natural OPA while the sliding behavior continues to be stable.
- Simulations of long-term (10 000 year and 1 million year) interaction between OPA fault gouge and CO_2-saturated brine (10–10^6 pore volumes) predict dissolution of micas (up to 5 wt%), a reduction of carbonate content (up to 5 wt%), and an increase of quartz (up to 20 wt%) and clay content (up to 20 wt%). These mineralogical changes are significant compared to brine-rock reactions, such as the conversion of illite to kaolinite, but they still do not significantly change fault frictional behavior. Our findings are consistent with experiments performed on unreacted and CO_2-exposed simulated fault gouges derived from material obtained from natural CO_2 reservoirs, such as the Entrada Sandstone (UT, USA) and the Röt Fringe Sandstone (Netherlands).
- Initial mineralogy of the fault gouge, and local variations thereof, imposes a stronger control on clay-rich fault behavior than the extent of CO_2-brine-rock interactions. For fluid-carrying components that may promote precipitation of substantial amounts of secondary minerals with drastically different frictional behavior, such as (swelling) clay minerals leading to an evolution from a clast-supported framework to a phyllosilicate-dominated matrix, or frictionally unstable minerals, like carbonates, the impact on frictional behavior is obviously more significant. As such, the ratio between quartz and carbonate plays a role in controlling frictional behavior, due to the promotion of thermally activated processes, leading to ductile behavior in the more intensely crushed brittle carbonate grains. However, in most typical CO_2 storage sites, a source of chemically different fluids leading to substantial mineralogical changes may be limited.
- Overall, mineralogical changes due to CO_2-brine-rock interactions can impact the frictional behavior and seismogenic potential of faults, and this can be assessed by the approach tested in this paper. However, it should be kept in mind that shear velocity, effective normal stress, and fault maturity, and internal fabric also remain important parameters, which cannot be neglected when assessing fault strength and stability.

Acknowledgements

We thank editor S. Ojo and three anonymous reviewers for their comments and suggestions, which helped to improve the manuscript. This research has been carried out in the context of the ULTimateCO_2-program. ULTimateCO_2 is a research program on Understanding the Long-Term fate of geologically stored CO_2 and is financially supported by the European Union (FP7). We thank Dr C. Nussbaum (Mont Terri Rock Laboratory) for providing the sample material and Dr M. Houben for helping with the SEM work. EB thanks ULTimateCO_2 for providing funding for the research. JPK's work was supported by the University of Wyoming School of Energy Resources and by a sabbatical leave from the University of Wyoming. SJTH performed the work within the *Future Energy and Resources Program* of the *Sustainability Research Theme* at Utrecht University.

References

1. Metz B, Davidson O, de Coninck H, Loos M and Meyer L, *IPCC Special Report on Carbon Dioxide Capture and Storage*. IPCC, Cambridge, UK (2005).
2. Gilfillan SMV, Lollar BS, Holland G, Blagburn D, Stevens S, Schoell M *et al*., Solubility trapping in formation water as dominant CO_2 sink in natural gas fields. *Nature* **458**(7238):614–618 (2009).
3. Al-Khdheeawi EA, Vialle S, Barifcani A, Sarmadivaleh M and Iglauer S, Influence of CO_2-wettability on CO_2 migration and trapping capacity in deep saline aquifers. *Greenhouse Gases: Sci Technol* **7**(2):328–338 (2017).
4. Al-Khdheeawi EA, Vialle S, Barifcani A, Sarmadivaleh M and Iglauer S, Impact of reservoir wettability and heterogeneity on CO_2-plume migration and trapping capacity. *Int J Greenhouse Gas Control* **58**:142–158 (2017).
5. Higgs KE, Haese RR, Golding SD, Schacht U and Watson MN, The Pretty Hill Formation as a natural analogue for CO_2 storage: An investigation of mineralogical and isotopic changes associated with sandstones exposed to low, intermediate and high CO_2 concentrations over geological time. *Chem Geol* **399**:36–64 (2015).
6. Kampman N, Bickle M, Wigley M and Dubacq B, Fluid flow and CO_2–fluid–mineral interactions during CO_2-storage in sedimentary basins. *Chem Geol* **369**:22–50 (2014).
7. White JA and Foxall W, Assessing induced seismicity risk at CO_2 storage projects: Recent progress and remaining

challenges. *Int J Greenhouse Gas Control* **49**:413–424 (2016).

8. Zoback MD and Gorelick SM, Earthquake triggering and large-scale geologic storage of carbon dioxide. *Proc Natl Acad Sci* **109**(26):10164–10168 (2012).
9. Cappa F and Rutqvist J, Seismic rupture and ground accelerations induced by CO_2 injection in the shallow crust. *Geophys J Int* **190**(3):1784–1789 (2012).
10. Vilarrasa V, Olivella S, Carrera J and Rutqvist J, Long term impacts of cold CO_2 injection on the caprock integrity. *Int J Greenhouse Gas Control* **24**:1–13 (2014).
11. Wang HF, *Theory of Linear Poroelasticity with Applications to Geomechanics and Hydrogeology*. Princeton University Press, Princeton, NJ (2000).
12. Sun Y, Aman M and Espinoza DN, Assessment of mechanical rock alteration caused by CO_2-water mixtures using indentation and scratch experiments. *Int J Greenhouse Gas Control* **45**:9–17 (2016).
13. Aman M, Espinoza DN, Ilgen AG, Major JR, Eichhubl P and Dewers TA, CO_2-induced chemo-mechanical alteration in reservoir rocks assessed via batch reaction experiments and scratch testing. *Greenhouse Gases: Sci Technol* **8**(1):133–149 (2018).
14. Major JR, Eichhubl P, Dewers TA, Urquhart AS, Olson JE and Holder J, The effect of CO_2-related diagenesis on geomechanical failure parameters: Fracture testing of CO_2-altered reservoir and seal rocks from a natural analog at Crystal Geyser, Utah. *48th US Rock Mechanics/Geomechanics Symposium*, Minneapolis, MN, USA, August 18. ARMA: American Rock Mechanics Association, pp. 1–5 (2014).
15. Alemu BL, Aagaard P, Munz IA and Skurtveit E, Caprock interaction with CO_2: A laboratory study of reactivity of shale with supercritical CO_2 and brine. *Appl Geochem* **26**(12):1975–1989 (2011).
16. Baines SJ and Worden RH, The long-term fate of CO_2 in the subsurface: natural analogues for CO_2 storage. *Geological Society, London, Special Publications* **233**(1):59–85 (2004).
17. Ikari MJ, Marone C and Saffer DM, On the relation between fault strength and frictional stability. *Geology* **39**(1):83–86 (2011).
18. Ikari MJ, Saffer DM and Marone C, Effect of hydration state on the frictional properties of montmorillonite-based fault gouge. *J Geophys Res* **112**(B6):B06423 (2007).
19. Tembe S, Lockner DA and Wong T-F, Effect of clay content and mineralogy on frictional sliding behavior of simulated gouges: Binary and ternary mixtures of quartz, illite, and montmorillonite. *J Geophys Res* **115**(B3):B03416 (2010).
20. Giorgetti C, Carpenter BM and Collettini C, Frictional behavior of talc-calcite mixtures. *J Geophys Res: Solid Earth* **120**(9):6614–6633 (2015).
21. Moore DE and Lockner DA, Frictional strengths of talc-serpentine and talc-quartz mixtures. *J Geophys Res: Solid Earth* **116**(B1):B01403 (2011).
22. Lu Z and He C, Frictional behavior of simulated biotite fault gouge under hydrothermal conditions. *Tectonophysics* **622**:62–80 (2014).
23. Verberne BA, Niemeijer AR, De Bresser JHP and Spiers CJ, Mechanical behavior and microstructure of simulated calcite fault gouge sheared at 20–600°C: Implications for natural faults in limestones. *J Geophys Res: Solid Earth* **120**(12):8169–8196 (2015).
24. Carpenter BM, Collettini C, Viti C and Cavallo A, The influence of normal stress and sliding velocity on the frictional behaviour of calcite at room temperature: insights from laboratory experiments and microstructural observations. *Geophys J Int* **205**(1):548–561 (2016).
25. Pluymakers AMH, Niemeijer AR and Spiers CJ, Frictional properties of simulated anhydrite-dolomite fault gouge and implications for seismogenic potential. *J Struct Geol* **84**:31–46 (2016).
26. Scuderi MM, Niemeijer AR, Collettini C and Marone C, Frictional properties and slip stability of active faults within carbonate–evaporite sequences: The role of dolomite and anhydrite. *Earth and Planetary Sci Lett* **369–370**:220–232 (2013).
27. Bakker E, Frictional and transport properties of simulated faults in CO_2 storage reservoirs and clay-rich caprocks [PhD thesis]. Utrecht University (2017).
28. Van Diggelen EWE, De Bresser JHP, Peach CJ and Spiers CJ, High shear strain behaviour of synthetic muscovite fault gouges under hydrothermal conditions. *J Struct Geol* **32**(11):1685–1700 (2010).
29. den Hartog SA, Saffer DM and Spiers CJ, The roles of quartz and water in controlling unstable slip in phyllosilicate-rich megathrust fault gouges. *Earth, Planets Space* **66**(1):78 (2014).
30. Whitney DL and Evans BW, Abbreviations for names of rock-forming minerals. *Am Mineral* **95**(1):185–187 (2010).
31. den Hartog SAM, Niemeijer AR and Spiers CJ, Friction on subduction megathrust faults: Beyond the illite–muscovite transition. *Earth and Planetary Sci Lett* **373**:8–19 (2013).
32. Logan JM and Rauenzahn KA, Frictional dependence of gouge mixtures of quartz and montmorillonite on velocity, composition and fabric. *Tectonophysics* **144**(1):87–108 (1987).
33. Samuelson J and Spiers CJ, Fault friction and slip stability not affected by CO_2 storage: Evidence from short-term laboratory experiments on North Sea reservoir sandstones and caprocks. *Int J Greenhouse Gas Control* **11S**:S78–S90 (2012).
34. Pluymakers AMH, Samuelson JE, Niemeijer AR and Spiers CJ, Effects of temperature and CO_2 on the frictional behavior of simulated anhydrite fault rock. *J Geophys Res: Solid Earth* **119**(12):2014JB011575 (2014).
35. Bakker E, Hangx SJT, Niemeijer AR and Spiers CJ, Frictional behaviour and transport properties of simulated fault gouges derived from a natural CO_2 reservoir. *Int J Greenhouse Gas Control* **54**(1):70–83 (2016).
36. Hangx S, Bakker E, Bertier P, Nover G and Busch A, Chemical–mechanical coupling observed for depleted oil reservoirs subjected to long-term CO_2-exposure – A case study of the Werkendam natural CO_2 analogue field. *Earth and Planetary Sci Lett* **428**:230–242 (2015).
37. Trippetta F, Collettini C, Barchi MR, Lupattelli A and Mirabella F, A multidisciplinary study of a natural example of a CO_2 geological reservoir in central Italy. *Int J Greenhouse Gas Control* **12**:72–83 (2013).
38. Rochelle CA, Czernichowski-Lauriol I and Milodowski AE, The impact of chemical reactions on CO_2 storage in geological formations: a brief review. *Geological Society, London, Special Publications* **233**(1):87–106 (2004).
39. Tembe S, Baud P and Wong T, Stress conditions for the propagation of discrete compaction bands in porous sandstone. *J Geophys Res* **113**(B9):B09409 (2008).

40. Niemeijer A, Marone C and Elsworth D, Fabric induced weakness of tectonic faults. *Geophys Res Lett* **37**(3):L03304 (2010).
41. Pearson FJ, Arcos D, Gaucher E and Waber HN. Chapter 5: Pore water chemistry and geochemical modelling, in *Mont Terri Project – Geochemistry of Water in the Opalinus Clay Formation at the Mont Terri Rock Laboratory*, ed. by Pearson FJ, Arcos D, Bath A, Boisson, Fernández AM, Gäbler H-E *et al.* Reports of the Federal Office for Water and Geology (FOWG), Geology Series. No. 5. Bern, Switzerland, pp. 67–104 (2003).
42. Bethke CM and Yeakel S, *The Geochemist's Workbench Release 10.0: Reaction Modeling Guide*. Aqueous Solutions, LLC, Champaign, IL (2014).
43. Chopping C and Kaszuba JP, Supercritical carbon dioxide-brine-rock reactions in the Madison Limestone of Southwest Wyoming: An experimental investigation of a sulfur-rich natural carbon dioxide reservoir. *Chem Geol* **322**:223–236 (2012).
44. Marcon V and Kaszuba JP, Carbon dioxide-brine-rock interactions in a carbonate reservoir capped by shale: Experimental insights regarding the evolution of trace metals. *Geochim Cosmochim Acta* **168**:22–42 (2015).
45. Hooper ECD, Fluid migration along growth faults in compacting sediments. *J Pet Geol* **14**:161–180 (1991).
46. Sibson RH, Fault-valve behavior and the hydrostatic-lithostatic fluid pressure interface. *Earth-Sci Rev* **32**(1):141–144 (1992).
47. Wiprut D and Zoback MD, Fault reactivation and fluid flow along a previously dormant normal fault in the northern North Sea. *Geology* **28**(7):595–598 (2000).
48. Faulkner D and Rutter E, Comparisons of water and argon permeability in natural clay-bearing fault gouge under high pressure at 20°C. *J Geophys Res* **105**(B7):16415–16426 (2000).
49. Moore DE and Lockner DA, Friction of the smectite clay montmorillonite, in *The Seismogenic Zone of Subduction Thrust Faults*, ed. by Dixon T and Moore C. Columbia University Press, New York, NY, pp. 317–345 (2007).
50. Marone C and Scholz CH, Particle-size distribution and microstructures within simulated fault gouge. *J Struct Geol* **11**(7):799–814 (1989).
51. Keulen N, Heilbronner R, Stünitz H, Boullier A-M and Ito H, Grain size distributions of fault rocks: A comparison between experimentally and naturally deformed granitoids. *J Struct Geol* **29**(8):1282–1300 (2007).
52. Niemeijer AR, Spiers CJ and Peach CJ, Frictional behaviour of simulated quartz fault gouges under hydrothermal conditions: Results from ultra-high strain rotary shear experiments. *Tectonophysics* **460**(1–4):288–303 (2008).
53. Ruina A, Slip instability and state variable friction laws. *J Geophys Res* **88**(B12):10359–10370 (1983).
54. Dieterich JH, Time-dependent friction and the mechanics of stick-slip. *Pageoph* **116**:790–806 (1978).
55. Dieterich JH, Modeling of rock friction: 2. Simulation of preseismic slip. *J Geophys Res* **84**(B5):2169–2175 (1979).
56. Scholz CH, Earthquakes and friction laws. *Nature* **391**:37–41 (1998).
57. Niemeijer AR and Vissers RLM, Earthquake rupture propagation inferred from the spatial distribution of fault rock frictional properties. *Earth Planet Sci Lett* **396**:154–164 (2014).
58. Yi F, Derek E, Chaoyi W and Yunzhong J, Mineralogical Controls on Frictional Strength, Stability, and Shear Permeability Evolution of Fractures. *J Geophys Res* **123**(5):3549–3563 (2018).
59. den Hartog SAM, Niemeijer AR and Spiers CJ, New constraints on megathrust slip stability under subduction zone P–T conditions. *Earth Planet Sci Lett* **353–354**:240–252 (2012).
60. Chen J, Verberne BA and Spiers CJ, Effects of healing on the seismogenic potential of carbonate fault rocks: Experiments on samples from the Longmenshan Fault, Sichuan, China. *J Geophys Res: Solid Earth* **120**(8):5479–5506 (2015).
61. Atkinson BK, Subcritical crack growth in geological materials. *J Geophys Res* **89**(B6):4077–4114 (1984).
62. Atkinson BK and Avdis V, Fracture mechanics parameters of some rock-forming minerals determined using an indentation technique. *International Journal of Rock Mechanics and Mining Sciences and Geomechanics Abstracts* **17**(6):383–386 (1980).
63. Kampman N, Busch A, Bertier P, Snippe J, Hangx S, Pipich V *et al.*, Observational evidence confirms modelling of the long-term integrity of CO_2-reservoir caprocks. *Nat Commun* **7** (12268) (2016).
64. Bossart P, Trick T, Meier PM and Mayor J-C, Structural and hydrogeological characterization of the excavation-disturbed zone in the Opalinus Clay (Mont Terri Project, Switzerland). *Appl Clay Sci* **26**(1):429–48 (2004).

Elisenda Bakker

Dr Elisenda Bakker is an energy and environmental consultant at Royal Haskoning DHV, where she gives advice on the physical and chemical processes that affect the mechanical and transport properties of rocks in the subsurface. She obtained her PhD from Utrecht University in 2016.

John Kaszuba

Dr John Kaszuba is an SER associate professor of geology and geophysics at the University of Wyoming. He is a recognized expert in high pressure/high temperature hydrothermal and multiphase fluid-rock reactions, integrating laboratory and computational approaches.

Sabine den Hartog

Dr Sabine den Hartog is a Lyell Research Fellow at Heriot-Watt University, Edinburgh. Her research focuses on the microscale mechanisms controlling fault frictional behavior, relevant to enhanced geothermal systems, carbon capture and storage, energy storage, and hydrofracturing operations.

Suzanne Hangx

Dr Suzanne Hangx is an assistant professor at the High Pressure and Temperature Laboratory at Utrecht University. She studies the physical and chemical processes controlling rock mechanical behavior in the subsurface in the context of CO_2/energy storage and geoenergy production.

Greenhouse Gas Sci Technol. **9**:19–36 (2019); DOI: 10.1002/ghg